Atmospheric controls on northeast Pacific temperature variability and change, 1900–2012

James A. Johnstone[a,1] and Nathan J. Mantua[a,b]

[a]Joint Institute for the Study of the Atmosphere and Ocean, University of Washington, Seattle, WA 98195; and [b]National Oceanic and Atmospheric Administration/National Marine Fisheries Service Southwest Fisheries Science Center, Santa Cruz, CA 95060

Edited by Ping Chang, Texas A&M University, College Station, TX, and accepted by the Editorial Board August 19, 2014 (received for review October 4, 2013)

Over the last century, northeast Pacific coastal sea surface temperatures (SSTs) and land-based surface air temperatures (SATs) display multidecadal variations associated with the Pacific Decadal Oscillation, in addition to a warming trend of ∼0.5–1 °C. Using independent records of sea-level pressure (SLP), SST, and SAT, this study investigates northeast (NE) Pacific coupled atmosphere–ocean variability from 1900 to 2012, with emphasis on the coastal areas around North America. We use a linear stochastic time series model to show that the SST evolution around the NE Pacific coast can be explained by a combination of regional atmospheric forcing and ocean persistence, accounting for 63% of nonseasonal monthly SST variance ($r = 0.79$) and 73% of variance in annual means ($r = 0.86$). We show that SLP reductions and related atmospheric forcing led to century-long warming around the NE Pacific margins, with the strongest trends observed from 1910–1920 to 1940. NE Pacific circulation changes are estimated to account for more than 80% of the 1900–2012 linear warming in coastal NE Pacific SST and US Pacific northwest (Washington, Oregon, and northern California) SAT. An ensemble of climate model simulations run under the same historical radiative forcings fails to reproduce the observed regional circulation trends. These results suggest that natural internally generated changes in atmospheric circulation were the primary cause of coastal NE Pacific warming from 1900 to 2012 and demonstrate more generally that regional mechanisms of interannual and multidecadal temperature variability can also extend to century time scales.

ocean–atmosphere coupling | Pacific climate | western US temperature | climate change

North Pacific climate observations since 1900 show evidence of multidecadal shifts between anomalous states of atmospheric circulation, sea surface temperature (SST), and adjacent land surface air temperature (SAT) and hydrology (1–4). These low-frequency climate fluctuations are often discussed together in the framework of the Pacific Decadal Oscillation (PDO), a climate pattern originally identified by refs. 4 and 2 as the leading empirical orthogonal function (EOF) of North Pacific monthly SST anomalies after subtraction of the global mean anomaly. The PDO varies over a range of monthly to multidecadal time scales, but is most notable for its tendency to switch phases every ∼20–30 y during the 20th century. Spatially, the PDO consists largely of an east-west anomaly dipole, reflecting a tendency for SSTs near the west coast of North America to vary in opposition to those in the central and western North Pacific.

Because the PDO index does not include the warming trend associated with global mean SST, it deviates from SST observations where century-long warming is substantial. In the northeast (NE) Pacific, for example, SSTs in the coastal California Current System warmed by 0.6–1 °C from 1900 to the early 2000s (5), and over the adjacent land margins, rising SATs have contributed to reductions in coastal low cloud frequency and mountain snow pack, with potentially negative implications for forest ecology and regional hydrology (6–8).

NE Pacific coastal SSTs, in connection to the PDO, vary in response to atmospheric forcing by the North Pacific Aleutian Low pressure cell, as well as remote forcing by the tropical El Niño-Southern Oscillation (ENSO) (9, 10). During warm ENSO conditions, the cyclonic circulation of the Aleutian Low typically strengthens, raising coastal SSTs by increasing net downward turbulent surface heat fluxes and reducing wind-driven vertical mixing, particularly in winter when winds are most vigorous (11–13). The dynamical origins of PDO variability are demonstrated by studies that have successfully reproduced the PDO index as a linear function of current Aleutian Low/ENSO forcing and SST persistence, explaining its temporal variability from monthly to multidecadal time scales (9, 10, 14, 15).

The role of these mechanisms in century-long temperature changes remain largely unknown, however, due to short analysis periods (10, 14) or, in longer-term studies, the use of detrended SSTs (9, 15). This study examines the coupled atmosphere–ocean history of the NE Pacific from 1900 to 2012, including trends, using a variety of data sources and established methods for describing coupled atmosphere–ocean variability. Physical mechanisms of atmosphere–ocean coupling are shown with reanalysis data that includes estimates of atmospheric winds and boundary layer conditions, turbulent and radiative surface heat fluxes, and upper ocean dynamics and thermal structure.

The study focuses primarily on SST variability within an area we term the NE Pacific Arc. The Arc corresponds closely to the eastern pole of the PDO, stretching around the North American coast from Alaska to California and offshore toward Hawaii (Fig. 1*A*). Additionally, long SAT records from coastal land stations are used as an independent source of temperature information to compare with temporal patterns in SST and atmospheric circulation.

Significance

Northeast Pacific coastal warming since 1900 is often ascribed to anthropogenic greenhouse forcing, whereas multidecadal temperature changes are widely interpreted in the framework of the Pacific Decadal Oscillation (PDO), which responds to regional atmospheric dynamics. This study uses several independent data sources to demonstrate that century-long warming around the northeast Pacific margins, like multidecadal variability, can be primarily attributed to changes in atmospheric circulation. It presents a significant reinterpretation of the region's recent climate change origins, showing that atmospheric conditions have changed substantially over the last century, that these changes are not likely related to historical anthropogenic and natural radiative forcing, and that dynamical mechanisms of interannual and multidecadal temperature variability can also apply to observed century-long trends.

Author contributions: J.A.J. and N.J.M. designed research, performed research, analyzed data, and wrote the paper.

The authors declare no conflict of interest.

This article is a PNAS Direct Submission. P.C. is a guest editor invited by the Editorial Board.

[1]To whom correspondence should be addressed. Email: jajstone@gmail.com.

This article contains supporting information online at www.pnas.org/lookup/suppl/doi:10.1073/pnas.1318371111/-/DCSupplemental.

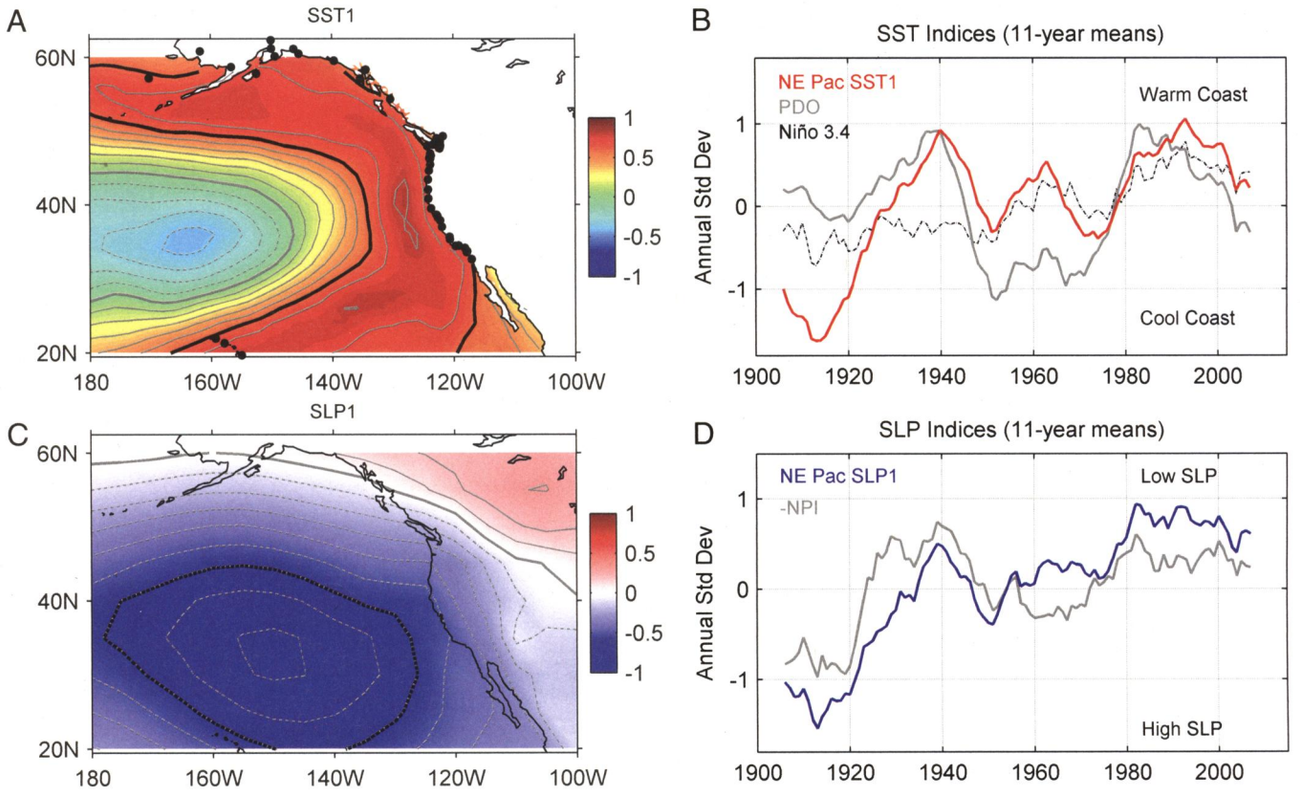

Fig. 1. Leading EOFs of monthly SST and SLP over the NE Pacific. (*A*) Correlations between SST EOF1 (SST1) time series and gridded SST anomaly series. Black dots mark the 51 long-term coastal SAT stations. (*B*) Eleven-year centered running means of NE Pacific SST1 (red), the North Pacific PDO (gray), and tropical Niño 3.4 SST (dashed). (*C*) SLP EOF 1 (SLP1) correlations with gridded SLP. (*D*) Eleven-year means of NE Pacific SLP1 (blue) and the North Pacific NPI (inverted, gray). Contour interval is 0.1; zero contours in bold; negative contours are dashed. Black bold contours enclose correlation magnitudes >0.6.

Past studies have noted a strong role for the NE Pacific atmosphere in SAT warming over the far western United States (6, 8, 16–19), whereas others have concluded that the magnitude of observed warming is inconsistent with natural climate variability (20–22). Here, we also document the strong influence of NE Pacific circulation change on observed SAT trends along the North American coastline and in the US Pacific coast states. To address the possible role of anthropogenic influences on NE Pacific circulation and temperature changes, we present output from an ensemble of climate model simulations run under a historical radiative forcing scenario for 1850–2005.

Leading Modes of NE Pacific SLP and SST

Empirical modes of NE Pacific (60°N–20°N, 180°W–100°W) SST and SLP variability were initially determined by separate EOF analyses of gridded normalized monthly anomalies for the 1900–2012 period. The primary SST data come from the 2°-gridded National Oceanic and Atmospheric Administration (NOAA) Extended Reconstruction SST dataset, version 3b (ERSST) (23). The leading SST mode (SST1) explains 30% of the total monthly variance, primarily reflecting coherent SST variations within an ~1,000-km–wide band around the NE Pacific coastal margins. This mode spatially resembles the PDO, but shows a stronger relationship to SSTs near the North American coast and a weaker connection to those in the central Pacific (Fig. 1*A*). The monthly SST1 time series correlates most strongly with local SST off northern California ($r = 0.82$ at 42°N, 128°W).

We formally define the NE Pacific Arc as the area within the study domain where local monthly SST correlations with SST1 exceed 0.6 (Fig. 1*A*). The time series of SST1 expansion coefficients is nearly identical (monthly $r > 0.99$) to an index of area-averaged SST anomalies within the Arc. This temperature index, SST_{ARC}, is used as a physically based metric of the statistical EOF pattern. A 1 SD (σ) anomaly of the SST1 index corresponds to an SST_{ARC} deviation of 0.46 °C, with individual monthly relationships deviating from this value by less than 10%. The monthly SST1 index is positively correlated with the PDO index (monthly $r = 0.53$), but displays considerably lower values before 1930, partly due to the absence of the global SST trend in the PDO index (Fig. 1*B*).

Primary SLP data come from the 5°-gridded National Center for Atmospheric Research (NCAR) monthly analysis (24), previously used in other studies of North Pacific low-frequency variability (1, 2, 25, 26). The leading mode of NE Pacific SLP (SLP1) explains 22% of overall variance, capturing coherent anomalies over the central NE Pacific and most of the study domain (Fig. 1*C*). The SLP1 index, oriented with positive values reflecting lower pressure, correlates most strongly with SLP NE of Hawaii (monthly $r = -0.84$) at 35°N, 150°W. These coordinates lie near the center of the summertime North Pacific High, so that SLP1 reflects variability of the subtropical anticyclone. In winter, the center of the pattern lies between the climatological centers of the Aleutian Low and North Pacific High, capturing southeastward extensions of the cyclonic Aleutian Low circulation. The SLP1 index displays a positive long-term trend, signifying SLP reductions over the NE Pacific from 1900 to 2012 (Fig. 1*D*). A comparison with the inverted North Pacific Index (NPI) of Aleutian SLP (27), developed from the same NCAR dataset indicates stronger relative SLP changes in the east than in the center of the North Pacific (Fig. 1*D*).

The SLP1 index (Fig. S1*A*) varies strongly on monthly time scales, producing a lag − 1 autocorrelation of 0.38, whereas greater

persistence in SST1 (Fig. S1*B*) yields a much higher autocorrelation of 0.91. The monthly correlation between the series ($r = 0.53$, detrended $r = 0.47$) far exceeds the 95% significance threshold, estimated by Monte Carlo simulation at ±0.17 (*Materials and Methods*). The correlation is maximized when the SLP1 index is smoothed with an 11-mo running mean and shifted backward in time to precede SST1 by 4 mo ($r = 0.76$; Fig. S1*C*). The strength of this tuned relationship suggests that the SST1 evolution is largely a time-integrated lagged ocean response to atmospheric forcing.

Time Series Model of Atmosphere–Ocean Coupling

The SLP1–SST1 relationship was further explored with a linear stochastic model (Eq. **1**) relating the SST1 index at each monthly time step t to a linear combination of SLP1-driven perturbations and SST persistence from the prior month t − 1. The model takes the form

$$SST_t = \alpha SST_{t-1} + \beta SLP_t + \varepsilon_t, \qquad [1]$$

where SST is the modeled SST1 index value, and SLP represents the normalized SLP1 time expansion coefficient. The terms α and β represent persistence and perturbation coefficients, respectively, and ε is a residual term. The model was initialized with the first SST1 value in January of 1900 (t = 1) and incrementally forced by the SLP1 anomaly for each of the next 1,355 mo through December 2012.

A sensitivity experiment identified model parameters $\alpha = 0.81$ and $\beta = 0.27$ (Fig. S1*D*), which are similar to those obtained from a linear regression of SST1(t) from SLP1(t) and SST1(t − 1) ($\alpha = 0.83$, $\beta = 0.21$). The stability of the model was tested by determining coefficients from two separate time intervals (1900–1956: $\alpha = 0.82$, $\beta = 0.27$; 1956–2012: $\alpha = 0.83$, $\beta = 0.28$) and using each set of coefficients to model SST1 over the independent data segment. The combined split-sample simulation was nearly identical ($r > 0.99$) to the overall simulation, indicating a consistent relationship between NE Pacific SLP and SST throughout the last century.

A model α-coefficient less than 1 indicates SST damping and regression of anomalies toward the mean in the absence of further atmospheric forcing. An example of short-term model behavior is shown in the inset of Fig. 2*A*, which illustrates the SST1 response to an abrupt 12-mo SLP1 anomaly of +1σ, approximating the magnitude and duration of atmospheric anomalies over a strong El Niño event. The SST response can be seen to decay nearly completely within a year of cessation of forcing (10).

The overall monthly correlation between actual and modeled SST1 series ($r = 0.79$, detrended $r = 0.77$) (Fig. 2*A*) is shared between low-frequency (>10 y, $r = 0.90$; Fig. S1*E*) and high-frequency variations (<10 y, $r = 0.69$; Fig. S1*F*). The correlation between annual means of modeled and observed indices of SST1 ($r = 0.86$, detrended $r = 0.83$; Fig. 2*B*) reflects a high degree of atmospheric control on SST variability from interannual to century scales and strong agreement between the independent SLP and SST datasets. The stability of the model and the strength of the SLP–SST relationship suggest that large-scale SST variability is controlled largely by short-term ocean responses to the atmosphere. The atmosphere displays prominent low-frequency variations, including a considerable trend over the last century that is approximately proportional to the observed warming.

SLP Forcing and Atmosphere–Ocean Responses

Physical responses to atmospheric forcing were examined through linear regressions of gridded and Arc-averaged variables onto the normalized monthly SLP1 index. Atmospheric responses were analyzed with monthly data from the 20th Century Reanalysis (20CR), version 2 (28), and ocean responses were based on the Simple Ocean Data Assimilation (SODA) reanalysis, version 2.2.4 (29).

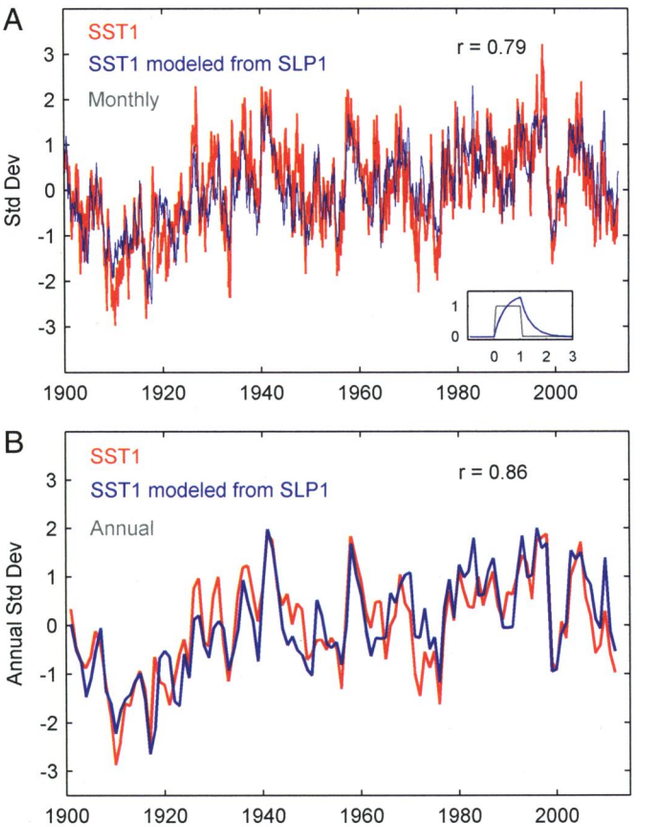

Fig. 2. NE Pacific SST1, modeled from SLP1. (*A*) Actual and modeled SST1 time series. (*Inset*) Modeled monthly SST1 response to a 12-mo +1σ anomaly of SLP1. (*B*) Annual (July–June) means of series in *A*.

A monthly +1σ SLP1 anomaly produces an SST tendency (ΔSST) that closely matches the SST1 spatial pattern (Fig. 3*A*), consistent with the strong correlation between the EOF indices. Warming tendencies of 0.05–0.15 °C occur throughout most of the Arc, with strongest responses observed off the California coast. With positive anomalies of SLP1, cyclonic surface wind anomalies over the NE Pacific (Fig. 3*B*) tend to reduce wind speeds over much of the Arc, weakening the mean westerlies in the north, the northerlies along the US coast, and the northeasterly trade winds in the subtropics. Net positive (downward) surface (sensible plus latent) turbulent heat flux anomalies respond in a form that resembles the SST response (Fig. 3*B*), suggesting a key role in the formation of the Arc pattern. Positive heat flux responses in the range of +5–+10 W/m^2 are seen throughout most of the Arc, with a maximum around +15 W/m^2 in the trade wind region northeast of Hawaii, where wind speed reductions are greatest.

SLP1 impacts on upper ocean thermal advection were estimated by calculating local SST gradient advection (°C/month) from zonal and meridional temperature gradients (°C/m) and velocities (m/s) at 5-m depth. The surface current response, illustrated by the vectors in Fig. 3*C*, reveals a pattern of anomalous meridional divergence from the central NE Pacific. Warm advection anomalies of +0.2 °C/mo are largest in areas of anomalous poleward flow in the far north, whereas comparable cooling occurs to the south with anomalous equatorward currents. Vertical temperature advection was similarly calculated across the upper ocean thermocline, defined by the maximum vertical temperature gradient at each location. Fig. 3*D* shows localized positive responses around +0.1 °C/mo, reflecting reductions in coastal

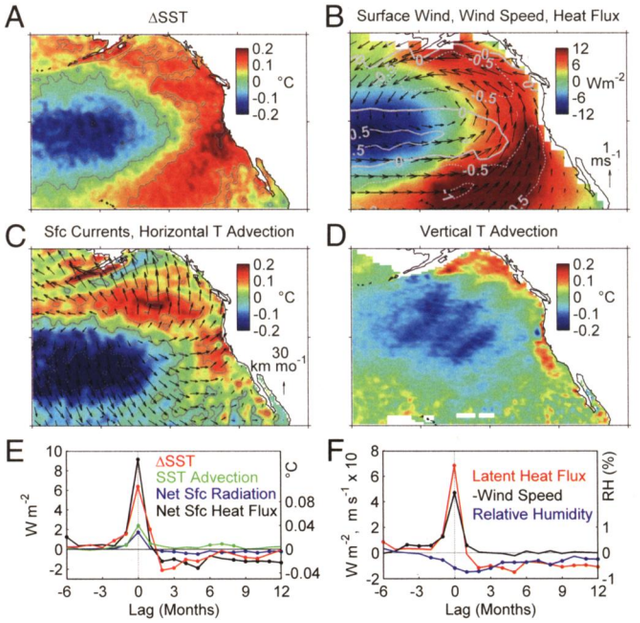

Fig. 3. NE Pacific responses to monthly +1σ SLP1 forcing, expressed as linear regression coefficients. (*A*) SODA 5-m temperature tendency (ΔSST). (*B*) 20CR 10-m winds (vectors), wind speeds (contours), and net downward turbulent surface heat fluxes (shading). (*C*) SODA surface (5-m) currents (vectors) and horizontal SST gradient advection (shading). (*D*) SODA vertical temperature gradient advection across the thermocline. (*E*) Leading and lagging regression responses of Arc-average indices: ΔSST, SST advection (SODA), and net radiation and surface heat flux (20CR). (*F*) Arc-average index responses of 20CR latent heat flux, 10-m wind speed, and 2-m relative humidity. Dotted lag-regression values indicate statistically significant ($P < 0.05$) responses.

upwelling, whereas negative responses in the open ocean correspond to areas of reduced downwelling and stronger winds, which promote greater entrainment of cool water from depth (13). Although SLP1 forcing generates upwelling-related temperature responses along the North American coast, only modest ($|r| \leq 0.3$) correlations were obtained with alongshore winds and published coastal upwelling indices (30).

Regressions calculated from Arc-averaged variables (Fig. 3 *E* and *F*) include simultaneous, as well as precursor and delayed responses in lagged regressions at −6 to +12 mo. A +1σ SLP1 anomaly produces a lag-zero SST tendency of +0.11 °C (Fig. 3*E*), simultaneous with a net downward increase in the turbulent heat flux (+9 W/m^2), and a smaller increase in net surface radiation (+2 W/m^2). Advective warming is estimated at +0.04 °C/mo, whereas the turbulent heat flux anomaly is equivalent to a temperature increase of 0.08 °C/mo over the Arc mean mixed layer depth of 75 m. Arc-averaged SODA subsurface temperatures respond to SLP1 with weaker amplitudes and larger delays than the SST, however, so that an assumption of uniform response by an upper ocean mixed layer is not fully realistic on monthly and longer time scales.

SLP1 regressions are consistent with model results showing that wind-driven heat fluxes are more important than advection in regulating NE Pacific SST (13). We find a small monthly correlation between anomalies of Arc-averaged turbulent heat flux and SST_{ARC} ($r = 0.10$), consistent with results from ref. 11 but considerably stronger heat flux relationships with the dynamical forcing represented by SLP1 ($r = 0.57$) and the monthly SST tendency (ΔSST_{ARC}, $r = 0.53$). Monthly SLP1 forcing tends to reduce the Arc-average wind speed (−0.5 m/s), reducing evaporation rates and increasing the net downward latent heat flux (+7 W/m^2).

Following peak warming by SLP1 wind forcing at lag zero, the ΔSST response turns negative as the forced SST anomaly decays over the next several months. At +2 to +5 mo, the SST decline is associated with reduced boundary layer (2 m) relative humidity and negative (i.e., upward) latent heat flux anomalies that signify greater evaporative cooling of the ocean surface. Positive Arc SST anomalies thus appear to be damped by a negative feedback that results from warming of the atmospheric boundary layer and the nonlinear increase of saturation specific humidity with temperature (31). SLP1 forcing initiates a sequence of processes that includes wind-driven SST anomalies and subsequent SST-driven damping, both largely produced through anomalous latent heat fluxes. The monthly wind forcing is considerably stronger, so that SST1 and SST_{ARC} closely track the evolution of SLP1.

Circulation-Driven Temperature Changes: 1900–2012

The strong covariation of NE Pacific SLP and SST presents a clear picture of circulation-driven temperature variability and change from 1900 to 2012 (Figs. 2 and 4). Early 20th century changes feature decadal trends from near-mean conditions in 1900 to historic anomalies of high pressure and low coastal SST from 1910 to 1920. Steep trends toward lower SLP and coastal warming then followed from 1920 to 1940. Relatively high SLP and cool coastal temperatures prevailed from 1945 to 1957 and from 1971 to 1976, surrounding a period of low pressure and coastal warmth from 1958 to 1970. Elevated temperatures from the late 1970s to the early 2000s appear to be consequences of persistently negative SLP anomalies over the NE Pacific that reduced wind speeds, thereby increasing the net downward turbulent heat flux and warm poleward SST advection over the NE Pacific Arc (13). Over the decade from 2003 to 2012, cooling occurred in conjunction with higher SLP, consistent with stronger winds, greater turbulent heat losses, and cool equatorward advection, leading to a partial reversal of century-long circulation and temperature trends.

An index of coastal SAT was also developed from 51 long-term stations around the NE Pacific margins (Fig. 1*A*). This index, SAT_{ARC}, provides further support for the ocean–atmosphere history depicted by marine observations, with a similar interannual and low-frequency evolution to SST1 ($r = 0.80$, detrended $r = 0.75$), SST_{ARC} ($r = 0.80$, detrended $r = 0.76$), and SLP1 ($r = 0.75$, detrended $r = 0.64$; Fig. 4). Arc SST changes in ERSST data are well constrained by direct observations (Fig. S2) and similarly represented by several other SST datasets (*SI Text* and Fig. S3). Among several SLP datasets, NCAR SLP exhibits the most consistent relationships with coastal temperatures on interannual and longer time scales (*SI Text* and Table S1). Low-frequency

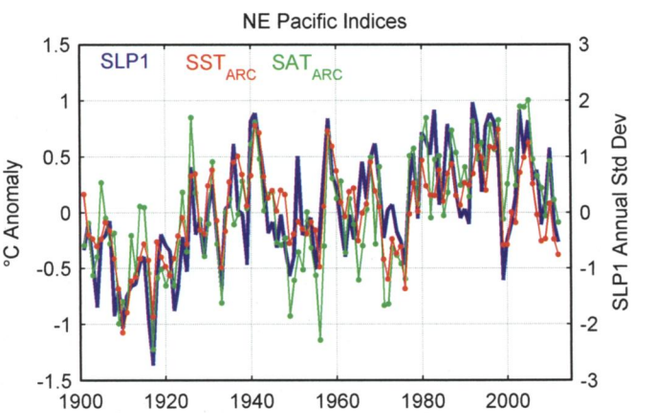

Fig. 4. NE Pacific climate indices: annual (July–June) means of SLP1, SST_{ARC}, and SAT_{ARC}.

changes in NCAR SLP have also been successfully linked with similar behavior in other North Pacific climate variables (1–3).

Summary and Discussion

Independent records of NE Pacific SLP, SST, and SAT provide consistent evidence for strong atmospheric regulation of coastal temperatures from monthly to century time scales and substantial ocean–atmosphere changes over the last century. Century-long warming of the NE Pacific Arc occurred in conjunction with regional SLP reductions that, based on their short-term influences, appear to account for much of the observed century-long warming trend as well.

When the influence of the annual SLP1 index is removed from coastal NE Pacific and western US temperature indices by linear regression, the 1901–2012 linear warming trends are strongly reduced (Table 1 and Fig. S4). The positive trend in SST_{ARC} is entirely accounted for by SLP1 circulation changes, and the trend in SAT_{ARC} is reduced by more than 80% when adjusted for SLP1 dynamics. SLP1 circulation anomalies account for more than 80% of SAT warming over the US Pacific coast states and more than 90% of warming over Washington, Oregon, and northern California, reducing the 1901–2012 trends to statistically insignificant ($P > 0.05$) levels. A significant warming trend remains over southern California, although reduced by more than 60%. Regional atmospheric forcing, understood as the primary driver of the PDO (10, 14), also accounts for nearly all (80–100%) of the observed SST and SAT warming around the coastal NE Pacific Arc and comparable fractions over the US Pacific coast states north of 37°N.

This high degree of dynamical control on long-term warming is consistent with results from studies of Cascade Range snowpack reduction (8) and earlier spring snow melt in California (6). Other studies have quantified smaller (≤50%) circulation influences (18, 32, 33) on western US warming, but in many cases dynamical forcing is inferred from detrended circulation proxies (33–36), including the PDO, or indices representing atmospheric conditions in the central North Pacific [e.g., the NPI (18, 33) or the Pacific-North American (PNA) pattern (32, 34)]. Detrended indices are unsuited to capture dynamical changes, and we find generally stronger coastal temperature relationships with NE Pacific SLP1 than with the NPI or PNA (Table S2).

To assess whether NE Pacific circulation trends might be attributed to changes in large-scale net radiative forcing, we compared observed SLP changes with those in CMIP5 historical global climate model (GCM) simulations (Fig. S5). Among 31 individual GCM simulations examined, each forced by the same natural and anthropogenic radiative forcings, none produced SLP changes that approached the observed −1.3-hPa change in NE Pacific SLP between the first and last 30 y of the 1900–2005 period. These results are consistent with other GCM studies showing mixed or weak SLP responses to anthropogenic net radiative forcing in the subtropical NE Pacific (37–40). In response to scenarios with increased anthropogenic radiative forcing over the course of the next century, some simulations depict an intensification and northward displacement of the Aleutian Low, but little systematic response in the subtropical NE Pacific (39, 40). Other studies, however, show slight tendencies for higher NE Pacific SLP (37, 38) and the negative phase of the PDO (41).

Recent GCM results from large-ensemble experiments (38) show that anthropogenically forced SLP changes in the NE Pacific are considerably weaker than natural internal variability over the 2010–2060 period. We find that CMIP5 GCM historical and 500+-y preindustrial control simulations generate realistic levels of interannual SLP variability in the NE Pacific but only 50–70% of observed low-frequency (decadal and longer) variability (Table S3). We conclude that internal variability is the most likely source of the observed SLP decline and that current GCMs may not adequately capture the underlying processes. It is also notable that the strongest changes in NE Pacific circulation and temperature occurred before 1940, when the combined natural and anthropogenic net radiative forcing changes are thought to be smaller than those in recent decades (42). Modest regional warming since 1940 and a possible reversal of long-term SLP and regional surface temperature trends between 1980 and 2012 suggest that low-frequency circulation changes in the NE Pacific have not responded in a robust linear manner to anthropogenic net radiative forcing.

The Intergovernmental Panel on Climate Change Fifth Assessment (AR5) Report (42) estimates that anthropogenic impacts have produced a 2-W/m^2 increase in the global average net radiative forcing between 1750 and 2011. A substantially greater +10-W/m^2 dynamical forcing of the net downward turbulent heat flux is inferred over the NE Pacific Arc from 1900 to 2012, based on the +9-W/m^2 monthly response to each +1σ anomaly of SLP1 and a +1.1σ linear change over this period. The impact of this direct heat flux forcing has likely been augmented by ocean advective processes and mitigated by negative feedbacks through boundary layer responses to the warming itself (31).

Atmospheric forcing of NE Pacific SST is well established on monthly to multidecadal time scales (10–12, 14, 25, 27). Based on the strong, physically realistic correlation between large-scale SLP and SST indices from 1900 to 2012, we conclude that dynamical forcing accounts for virtually all of the observed warming in NE Pacific Arc SST over the 1900–2012 period as well. Tree-ring proxies of the PDO pattern and NE Pacific coastal SST also display evidence of century-long trends during the last several hundred years (43–46). Further study may clarify the mechanisms behind the low-frequency circulation-temperature variability of the NE Pacific, so that a fuller understanding of natural and anthropogenic changes can be attained.

Table 1. NE Pacific temperature trends

Temperature index	Original	SLP1	SLP1 residuals
SST_{ARC}	0.47*	0.53*	−0.06
SAT_{ARC}	0.81*	0.66*	0.14
Western US SAT	0.75*	0.62*	0.13
Washington SAT	0.69*	0.66*	0.03
Oregon SAT	0.67*	0.64*	0.02
Northern California SAT	0.53*	0.51*	0.02
Southern California SAT	1.13*	0.69*	0.44*

Linear temperature trends (°C/century) for NE Pacific and western US regions (July–June annual means,1901–2012). Original trends, trends predicted by SLP1 based on linear regression, and trends of SLP1 regression residuals (Fig. S4).

*Statistically significant ($P < 0.05$) values.

Materials and Methods

The primary SST data for this study consist of monthly 2°-gridded and fully interpolated fields from the ERSST (23). Primary SLP data come from the monthly NCAR Northern Hemisphere 5° analysis (24). The NCAR SLP dataset is a quality-controlled compilation of daily surface map analyses from various sources. Comparisons with other SST and SLP datasets are illustrated in Fig. S3.

To objectively isolate large-scale modes of NE Pacific variability, EOF analysis was first performed separately on normalized monthly matrices of SLP and SST. The primary modes in each field were then compared, first by correlation, with statistical significance estimated from a Monte Carlo simulation using synthetic random SLP1 series with observed levels of autocorrelation and low-frequency variance. A stochastic time series model was created to estimate the monthly SST1 response to a combination of SLP1 forcing and monthly lag − 1 SST persistence, an approach originally developed in ref. 47 and applied in ref. 48 to describe atmospheric forcing of the extratropical oceans. This method has been used successfully to explain the evolution of the PDO (9, 10, 14, 15), although none of these prior studies have included the century-long trends

in North Pacific circulation and SST. Monthly SLP1, SST1, SST_{ARC}, and SAT_{ARC} indices are included in Dataset S1.

Monthly atmospheric and surface data obtained from 20CR (1900–2012) include net turbulent heat fluxes (both latent and sensible), surface radiation (solar and longwave, upward and downward), near-surface (10-m height) winds, boundary-layer (2-m height) temperature, and specific humidity (used to calculate relative humidity). Upper ocean dynamical and thermal advective responses from SODA (1900–2008), which is forced with 20CR surface winds, include near-surface (5-m depth) temperatures and horizontal currents and subsurface temperatures and vertical velocities.

Linear regression was used to estimate monthly responses to a $+1\sigma$ anomaly of the leading pressure mode SLP1. Regressions were performed on monthly indices over the 1920–2008 period during which both datasets are available and 20CR circulation variability agrees well with the primary NCAR SLP dataset (*SI Text*). Because century-long trends in 20CR heat fluxes and SODA advection depart substantially from observed SST changes, regressions were performed on indices treated with a 120-mo high-pass Hamming filter, capturing the short-term responses reflected in the time series model. Statistical significance was determined from Monte Carlo simulations using random, identically filtered SLP1 series matching the observed level of lag − 1 autocorrelation. Anomaly responses were computed separately for each calendar month, and the overall responses were estimated as the annual means of the monthly regression coefficients.

SATs around the NE Pacific margin were investigated with monthly station data from the US Historical Climate Network, version 2 (USHCNv2) (49) and the Global Historical Climate Network, version 3 (GHCNv3) (50), using adjusted versions of both datasets. A NE Pacific Arc SAT index (SAT_{ARC}) was constructed from all 51 USHCNv2 and GHCNv3 coastal stations with at least 960 mo of available data (Fig. 1*A*). Monthly anomaly series were first calculated for subregions of coastal Alaska (12 stations), British Columbia (3), Washington-Oregon (19), California (14), and Hawaii (3). For each station, missing data were infilled by monthly regression from up to three nearest neighbors, defined by correlation coefficient. A small number of remaining missing subregional estimates were filled by regression on neighboring subregions. The final SAT_{ARC} index was calculated as the unweighted mean of the five subregional series, expressed in monthly degree Celcius anomalies with respect to the full 1900–2012 period. Temperature indices were similarly constructed for the US Pacific coast states, using all USHCNv2 stations to produce monthly anomaly series for Washington, Oregon, and northern and southern California, the latter divided at 37°N.

1. Deser C, Phillips AS, Hurrell JW (2004) Pacific interdecadal climate variability: Linkages between the tropics and the North Pacific during boreal winter since 1900. *J Clim* 17(16):3109–3124.
2. Mantua NJ, Hare SR, Zhang Y, Wallace JM, Francis RC (1997) A Pacific interdecadal climate oscillation with impacts on salmon production. *Bull Am Meteorol Soc* 78(6):1069–1079.
3. Minobe S (1997) A 50-70 year climatic oscillation over the North Pacific and North America. *Geophys Res Lett* 24(6):683–686.
4. Zhang Y, Wallace JM, Battisti DS (1997) ENSO-like interdecadal variability: 1900-93. *J Clim* 10(5):1004–1020.
5. Field D, Cayan D, Chavez F (2006) Secular warming in the California current and North Pacific. *CCOFI Rep* 47:92–108.
6. Dettinger MD, Cayan DR (1995) Large-scale atmospheric forcing of recent trends toward early snowmelt runoff in California. *J Clim* 8(3):606–623.
7. Johnstone JA, Dawson TE (2010) Climatic context and ecological implications of summer fog decline in the coast redwood region. *Proc Natl Acad Sci USA* 107(10): 4533–4538.
8. Stoelinga MT, Albright MD, Mass CF (2010) A new look at snowpack trends in the Cascade Mountains. *J Clim* 23(10):2473–2491.
9. Newman M, Compo GP, Alexander MA (2003) ENSO-forced variability of the Pacific decadal oscillation. *J Clim* 16(23):3853–3857.
10. Schneider N, Cornuelle BD (2005) The forcing of the Pacific decadal oscillation. *J Clim* 18(21):4355–4373.
11. Cayan DR (1992) Latent and sensible heat flux anomalies over the northern oceans: Driving the sea surface temperature. *J Phys Oceanogr* 22(8):859–881.
12. Cayan DR (1992) Latent and sensible heat flux anomalies over the northern oceans: The connection to monthly atmospheric circulation. *J Clim* 5(4):354–369.
13. Miller AJ, Cayan DR, Barnett TP, Graham NE, Oberhuber JM (1994) Interdecadal variability of the Pacific-ocean: Model response to observed heat-flux and wind stress anomalies. *Clim Dyn* 9(6):287–302.
14. Chhak KC, Di Lorenzo E, Schneider N, Cummins PF (2009) Forcing of low-frequency ocean variability in the northeast Pacific. *J Clim* 22(5):1255–1276.
15. Shakun JD, Shaman J (2009) Tropical origins of North and South Pacific decadal variability. *Geophys Res Lett* 36(19):L19711.
16. Cayan DR, Kammerdiener SA, Dettinger MD, Caprio JM, Peterson DH (2001) Changes in the onset of spring in the western United States. *Bull Am Meteorol Soc* 82(3): 399–415.
17. Favre A, Gershunov A (2006) Extra-tropical cyclonic/anticyclonic activity in North-Eastern Pacific and air temperature extremes in Western North America. *Clim Dyn* 26(6):617–629.
18. Mote PW (2003) Trends in temperature and precipitation in the Pacific Northwest during the twentieth century. *Northwest Sci* 77(4):271–282.
19. Stewart IT, Cayan DR, Dettinger MD (2005) Changes toward earlier streamflow timing across western North America. *J Clim* 18(8):1136–1155.
20. Barnett TP, et al. (2008) Human-induced changes in the hydrology of the western United States. *Science* 319(5866):1080–1083.
21. Bonfils C, et al. (2008) Detection and attribution of temperature changes in the mountainous western United States. *J Clim* 21(23):6404–6424.
22. Pierce DW, et al. (2008) Attribution of declining western US snowpack to human effects. *J Clim* 21(23):6425–6444.
23. Smith TM, Reynolds RW, Peterson TC, Lawrimore J (2008) Improvements to NOAA's historical merged land-ocean surface temperature analysis (1880-2006). *J Clim* 21(10): 2283–2296.
24. Trenberth KE, Paolino JA (1980) The Northern Hemisphere sea-level pressure data set: Trends, errors and discontinuities. *Mon Weather Rev* 108(7):855–872.
25. Trenberth KE (1990) Recent observed interdecadal climate changes in the Northern Hemisphere. *Bull Am Meteorol Soc* 71(7):988–993.
26. Trenberth KE, Paolino DA (1981) Characteristic patterns of variability of sea level pressure in the Northern Hemisphere. *Mon Weather Rev* 109(6):1169–1189.
27. Trenberth KE, Hurrell JW (1994) Decadal atmosphere-ocean variations in the Pacific. *Clim Dyn* 9(6):303–319.
28. Compo GP, et al. (2011) The twentieth century reanalysis project. *Q J R Meteorol Soc* 137(654):1–28.
29. Carton JA, Giese BS (2008) A reanalysis of ocean climate using Simple Ocean Data Assimilation (SODA). *Mon Weather Rev* 136(8):2999–3017.
30. Schwing FBM, O'Farrell M, Steger J, Baltz K (1996) Coastal upwelling indices, west coast of North America, 1946-1995. *NOAA Technical Memorandum NOAA-TM-NMFS-SWFC-231* (US Dept. of Commerce, Pacific Grove, CA).
31. Park S, Deser C, Alexander MA (2005) Estimation of the surface heat flux response to sea surface temperature anomalies over the global oceans. *J Clim* 18(21):4582–4599.
32. Abatzoglou JT (2011) Influence of the PNA on declining mountain snowpack in the Western United States. *Int J Climatol* 31(8):1135–1142.
33. Mote PW (2006) Climate-driven variability and trends in mountain snowpack in western North America. *J Clim* 19(23):6209–6220.
34. Abatzoglou JT, Rupp DE, Mote PW (2014) Seasonal climate variability and change in the Pacific Northwest of the United States. *J Clim* 27(5):2125–2142.
35. Hamlet AF, Mote PW, Clark MP, Lettenmaier DP (2005) Effects of temperature and precipitation variability on snowpack trends in the western United States. *J Clim* 18(21):4545–4561.
36. Mote PW, Hamlet AF, Clark MP, Lettenmaier DP (2005) Declining mountain snowpack in western North America. *Bull Amer Meterol Soc* 86(1):39–49.
37. Deser C, Phillips A, Bourdette V, Teng H (2012) Uncertainty in climate change projections: The role of internal variability. *Clim Dyn* 38(3-4):527–546.
38. Deser C, Phillips AS, Alexander M, Smoliak BV (2014) Projecting North American climate over the next 50 years: Uncertainty due to internal variability. *J Clim* 27(6): 2271–2296.
39. Oshima K, Tanimoto Y, Xie S-P (2012) Regional patterns of wintertime SLP change over the North Pacific and their uncertainty in CMIP3 multi-model projections. *J Meteorol Soc Jpn* 90A:385–396.
40. Salathé EP Influences of a shift in North Pacific storm tracks on western North American precipitation under global warming. *Geophys Res Lett* 33(19):L19820.
41. Lapp SL, St Jacques J-M, Barrow EM, Sauchyn DJ (2011) GCM projections for the Pacific Decadal Oscillation under greenhouse forcing for the early 21st century. *Int J Climatol* 32(9):1423–1442.
42. Myhre G, et al. (2013) *Climate Change 2013: The Physical Science Basis. Contribution of Working Group I to the Fifth Assessment Report of the Intergovernmental Panel on Climate Change*, eds Stocker TF, et al. (Cambridge Univ Press, Cambridge, UK).
43. D'Arrigo R, et al. (2005) Tropical-North Pacific climate linkages over the past four centuries. *J Clim* 18(24):5253–5265.
44. MacDonald GM, Case RA (2005) Variations in the Pacific Decadal Oscillation over the past millenium. *Geophys Res Lett* 32(8):L08703.
45. Wiles GC, D'Arrigo RD, Jacoby GC (1998) Gulf of Alaska atmosphere-ocean variability over recent centuries inferred from coastal tree-ring records. *Clim Change* 38(3): 289–306.
46. Wilson R, Wiles G, D'Arrigo R, Zweck C (2007) Cycles and shifts: 1,300 years of multidecadal temperature variability in the Gulf of Alaska. *Clim Dyn* 28(4):425–440.
47. Hasselmann K (1976) Stochastic climate models. 1. Theory. *Tellus* 28(6):473–485.
48. Frankignoul C, Hasselmann K (1977) Stochastic climate models. 2. Application to sea-surface temperature anomalies and thermocline variability. *Tellus* 29:289–305.
49. Menne MJ, Williams CN, Vose RS (2009) The United States Historical Climatology Network monthly temperature data: Version 2. *Bull Am Meteorol Soc* 90(7):993–1007.
50. Lawrimore JH, et al. (2011) An overview of the Global Historical Climatology Network monthly mean temperature data set, version 3. *J Geophys Res Atmos* 116:D19121.